Available online at www.sciencedirect.com
ScienceDirect
Journal of the European Ceramic Society 31 (2011) 501–506
www.elsevier.com/locate/jeurceramsoc

Effect of processing method on physical properties of Nb_2O_5

M.R.N. Soares [a], S. Leite [a], C. Nico [a], M. Peres [a], A.J.S. Fernandes [a], M.P.F. Graça [a], M. Matos [b], R. Monteiro [b], T. Monteiro [a], F.M. Costa [a,*]

[a] *Departamento de Física e i3N, Universidade de Aveiro, 3810-193 Aveiro, Portugal*
[b] *KEMET Electronics Portugal, Évora, Portugal*

Received 8 July 2010; received in revised form 30 September 2010; accepted 13 October 2010
Available online 20 November 2010

Abstract

Samples of Nb_2O_5 were prepared by laser floating zone (LFZ) technique and by solid-state reaction in order to study some of their physical properties as a function of synthesis conditions. Single crystals fibres were obtained by LFZ, while a structural orthorhombic to monoclinic phase transition was observed in samples sintered at temperature higher than 800 °C. Transmission optical spectroscopy and photoconductivity measurements allowed identifying a ~3.2 eV bandgap energy for the H-Nb_2O_5 monoclinic crystalline phase. Band gap shrinkage of ~100 meV was observed from 14 K to RT. For the orthorhombic phase (T-Nb_2O_5), the photoconductivity measurements evidence a higher energy bandgap. The sintered samples have shown a broad recombination luminescence band at the orange/red spectral region while no luminescence was detected from the LFZ grown fibres. A dielectric constant of ~40 was found for the 800 °C and 1200 °C sintered pellets while that of 1000 °C reached four times that value.

Keywords: D. Niobates; B. Fibres; C. Optical properties; C. Dielectric properties; Laser Floating Zone

1. Introduction

Niobium oxide based materials are very attractive for electronic applications, particularly the niobium pentoxide, Nb_2O_5, the most stable of the niobium oxides. Nb_2O_5 evidences a set of physical properties which are very important for its use in electronic passive components such as dielectric constant (ε') of 41[1] and a reported band gap of ~3.4–5.3 eV.[1] Recently, this material has also been appointed as a substitute of tantalum pentoxide ($\varepsilon' = 27$) for application in solid state capacitors.[2,3] Envisaging technological applications of Nb_2O_5, a deep knowledge of the conditions for each phase formation as well as their properties is absolutely necessary, since niobium pentoxide is a polymorphic material exhibiting different crystalline phases.[4,5] The main phases reported in literature for Nb_2O_5 are T-Nb_2O_5, and H-Nb_2O_5.[6] The T-Nb_2O_5 is the lowest temperature phase with orthorhombic crystalline structure ($a = 6.17$ Å; $b = 29.32$ Å; $c = 3.94$ Å), the H-Nb_2O_5 being the most stable phase ocurring at high temperatures, with a monoclinic structure ($a = 21.20$ Å, $b = 3.82$ Å, $c = 19.39$ Å and $\beta = 120°10'$).[7] The formation conditions of each one of the Nb_2O_5 structures are strongly dependent on the heat treatment conditions, processing methods, starting materials, etc.[6]

The different crystalline structures of Nb_2O_5 can be described as NbO_6 octahedra shared in different ways. The T-Nb_2O_5 phase consists in 4×4 blocks of corner-shared NbO_6 octahedra, each connected block sharing the edges of the octahedron. The most stable structure, H-Nb_2O_5, has a shear structure consisting in 3×5 and 3×4 blocks of NbO_6 octahedra sharing the corners in their own block, and edges with octahedra in other blocks. Edge-shared octahedra exhibit large distortions that result in significant variations in Nb–O lengths, in opposition to corner-shared octahedra which are not significantly distorted.[8,9]

In this work, Nb_2O_5 materials were prepared by two different routes: (i) solid state reaction at different sintering temperatures (600–1200 °C) and (ii) Laser Floating Zone (LFZ) at different pulling rates (20 and 150 mm/h), a powerful technique to grow high melting temperature oxide crystals like Nb_2O_5 (1500 °C melting temperature)[10] at high pulling rates.[11] A detailed structural, morphological, optical, electrical and electro-optical comparative characterization of Nb_2O_5 samples was made taking into account the two distinct processing routes.

* Corresponding author.
E-mail address: flor@ua.pt (F.M. Costa).

0955-2219/$ – see front matter © 2010 Elsevier Ltd. All rights reserved.
doi:10.1016/j.jeurceramsoc.2010.10.024

2. Experimental details

Commercial Nb_2O_5 powder (Merck, 99.9%) was used as a starting material for both techniques. In the samples prepared by solid-state reaction, the Nb_2O_5 powder was pressed into pellets form (Ø 5 mm; $h \sim 1.2$ mm) using a uniaxial hydraulic press. The ceramic pellets were sintered in air at different temperatures: 600 °C, 800 °C, 900 °C, 1000 °C, 1100 °C and 1200 °C for 4 h with a rate temperature of 5 °C/min.

The feed and seed rods used in LFZ growth were prepared by a cold extrusion process. A small amount of polyvinyl alcohol (PVA) aqueous solution (0.1 kg/l) was mixed with Nb_2O_5 powder as a bonding agent to further extrusion into cylindrical bars with ~1.5 mm in diameter. A CO_2 laser (200 W, $\lambda = 10.6$ μm) was used in this work to grow the Nb_2O_5 fibres. Two pulling rates were studied (20 and 150 mm/h), the feeding to pulling rate ratio being kept at 2. The growth was directed downwards while rotating at 5 rpm both seed and feed rods. The laser power was maintained at 23 W.

The sintered pellets and as-grown fibres were structurally characterized by high resolution X-ray diffraction and Raman spectroscopy. The fibres were milled into powders so it was possible to analyze them by powder XRD. The XRD patterns of the pellets and milled fibres were obtained by an X'Pert MPD Philips difractometer (Cu Kα radiation, $\lambda = 1.54056$ Å). UV micro-Raman spectroscopy measurements were performed at room temperature in backscattering geometry, with a 325 nm He–Cd laser line using a HR-800 Jobin Yvon (Horiba) spectrometer. The microstructure of the pellets and polished longitudinal sections of the fibres were analysed by SEM on a Hitachi S4100-1, in secondary electron mode.

Steady state photoluminescence (PL) between 14 K and RT was measured using the same He–Cd laser as excitation source. The emitted light was dispersed by a Spex 1704 monochromator (1 m, 1200 mm^{-1}) fitted with a cooled Hamamatsu R928 photomultiplier. Unpolarized temperature dependent absorption measurements were performed using a tungsten lamp, the transmitted light being analysed using the same experimental set up described for the PL measurements. In addition, RT absorption spectra using a Jasco V-560 instrument were collected from sintered pellets. RT photoconductivity (PC) measurements were accomplished in contacted samples using a Xe lamp. The light beam was dispersed by a monochromator before reaching the sample. The bias voltage was applied using a Keithley 617 unit for the conductivity measurements.

The electrical characterization was made from 80 K to 360 K by impedance spectroscopy (40 Hz to 110 MHz) using an Agilent 4294A Precision Impedance Analyser in Cp-Rp configuration, while DC conductivity (σ_{dc}) measurements using an Electrometer Keithley 617 were also performed.

3. Results and discussion

Fig. 1 shows the XRD and Raman data taken from the Nb_2O_5 samples prepared by distinct routes under different processing conditions. The commercial powder used as starting material presents the orthorhombic T-Nb_2O_5, the same crystalline phase identified for the samples sintered at 600 °C and 800 °C. This structure crystallized in *Pbam* space group (D_{2h} point group) with the lattice parameters described in Table 1. For temperatures higher than 800 °C the diffraction patterns are assigned to the monoclinic phase, H-Nb_2O_5 which crystallizes in the *P*2 space group (C_2 point group). These indexations and crystallographic parameters were based on the JCPDS database. For the highest sintering temperatures (1000 °C, 1100 °C and 1200 °C) the H-phase remains the only crystalline phase, and an improvement of its crystalline quality is observed.The XRD analysis of fibres pulled at distinct rates shows the same monoclinic high temperature crystalline phase, H-Nb_2O_5, as the samples sintered at high temperatures. However, despite a single phase nature was observed for the slowest fibre, a minority NbO_2 phase on the fibre grown at the fastest rate was observed in the XRD analysis, though with very low intensity. Nevertheless, no effect of pulling rate was observed in the lattice parameters of H-Nb_2O_5 crystals in both fibres, Table 1.

The evolution of the crystalline phases formation with the sintering temperature was corroborated by the Raman spectra shown in Fig. 1(b). The bands between 200 cm^{-1} and 300 cm^{-1} are characteristic of the bending modes of Nb–O–Nb bonds in the orthorhombic phase.[11] For temperatures below 800 °C, the main vibrational mode appear at 685 cm^{-1} which has been assigned to the vibrations of niobium polyhedrons in the orthorhombic phase.[12] For samples sintered above 900 °C, which exhibit the monoclinic phase H-Nb_2O_5, a new set of vibrational modes are observed. The most prominent bands in the monoclinic phase occur at higher frequencies, 991 cm^{-1} and 903 cm^{-1} and have been assigned to the edge-shared octahedra and corner shared NbO_6 octahedra vibrations.[4] At lower frequencies, Balachandran et al.[4] have reported vibrational modes in the same frequency range to the ones detected in the present work for the H-Nb_2O_5 structures. As expected, the vibrational spectra of the LFZ grown fibres and pellets sintered at high temperatures are identical, Fig. 1(b).

The SEM analysis of the samples prepared in this study show different morphological characteristics according to the processing route and sintering temperature as indicated in Fig. 2. The major difference is observed between the samples prepared by solid-state reaction, which are polycrystalline, and the fibres grown by LFZ, where no grain boundaries were observed, as expected in single crystals. However, the fibre pulled at higher growth rate presented the H-Nb_2O_5 and NbO_2 phases (as observed in the XRD analysis), disclosing crystalline imperfections possibly linked to inclusions. Moreover, the samples sintered up to 800 °C, with an orthorhombic T-Nb_2O_5 crystalline phase, exhibit nearly spherical grains, whose size increases with the sintering temperature due to coalescence. A noteworthy change in grain morphology is clearly seen for samples sintered at 900 °C and above. Here, when the H-Nb_2O_5 crystalline phase is present, elongated grains with a parallelepiped geometry developed. The size of these polyhedral grains increases with the sintering temperature.Despite the fibres grown at 20 and 150 mm/h exhibit the same crystalline phase, according to the XRD and Raman data, the slower one is transparent and colourless, while the fastest is transparent and blue. The blue

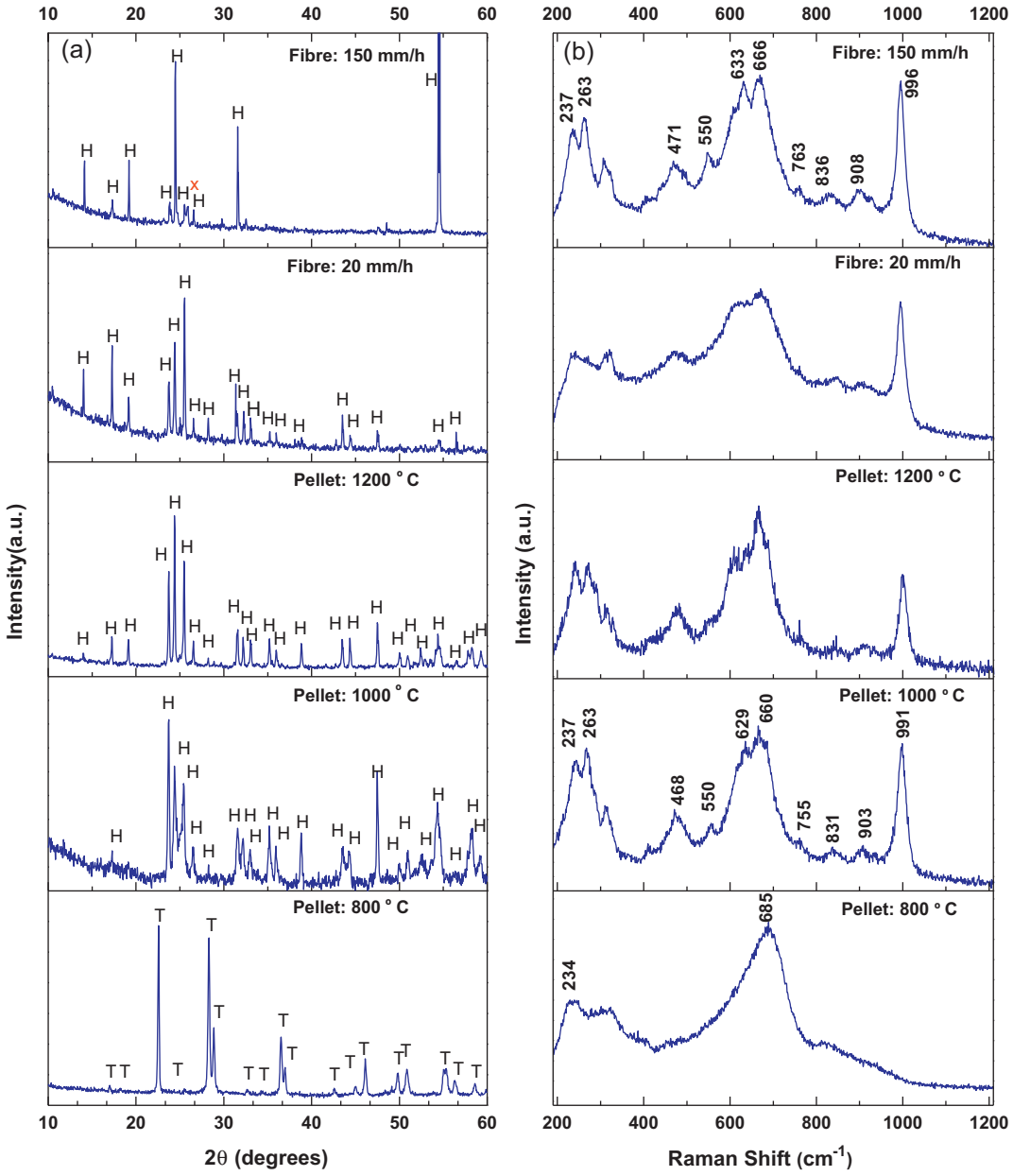

Fig. 1. (a) XRD diffraction patterns of the sintered Nb_2O_5 pellets and LFZ grown fibres (T – orthorhombic phase of Nb_2O_5; H – monoclinic phase of Nb_2O_5; x – NbO_2 phase). (b) Raman spectra of the same set of samples obtained at RT in backscattering configuration with the 325 nm laser line.

colour of some oxide fibres grown by floating-zone processes, e.g. TiO_2, has been associated to oxygen vacancies due to low oxygen partial pressure.[12,13] As referred, the fibre grown at the fastest rate presents a minority NbO_2 phase which could explain the origin of the blue colour, once the oxygen pressure was the same in both cases (the only variable was the growth rate). On the other hand, a pulling rate increase implies a concomitant increase in cooling rate during the crystallization process and,

Table 1
Structural properties of pellets and fibres.

Sample	Structure	Space group	Point group	Lattice parameters					
				a (Å)	*b* (Å)	*c* (Å)	*α* (°)	*β* (°)	*γ* (°)
Pellets: 600 °C and 800 °C	Orthorhombic	*Pbam*	D_{2h}	6.17	3.94	29.31	90.0	90.0	90.0
Pellets: 900 °C at 1200 °C	Monoclinic	*P*2	C_2	21.15	3.82	19.35	90.0	119.8	90.0
Fibre: 20 mm/h	Monoclinic	*P*2	C_2	20.37	3.82	19.36	90.0	115.72	90.0
Fibre: 150 mm/h	Monoclinic	*P*2	C_2	20.37	3.82	19.36	90.0	115.75	90.0

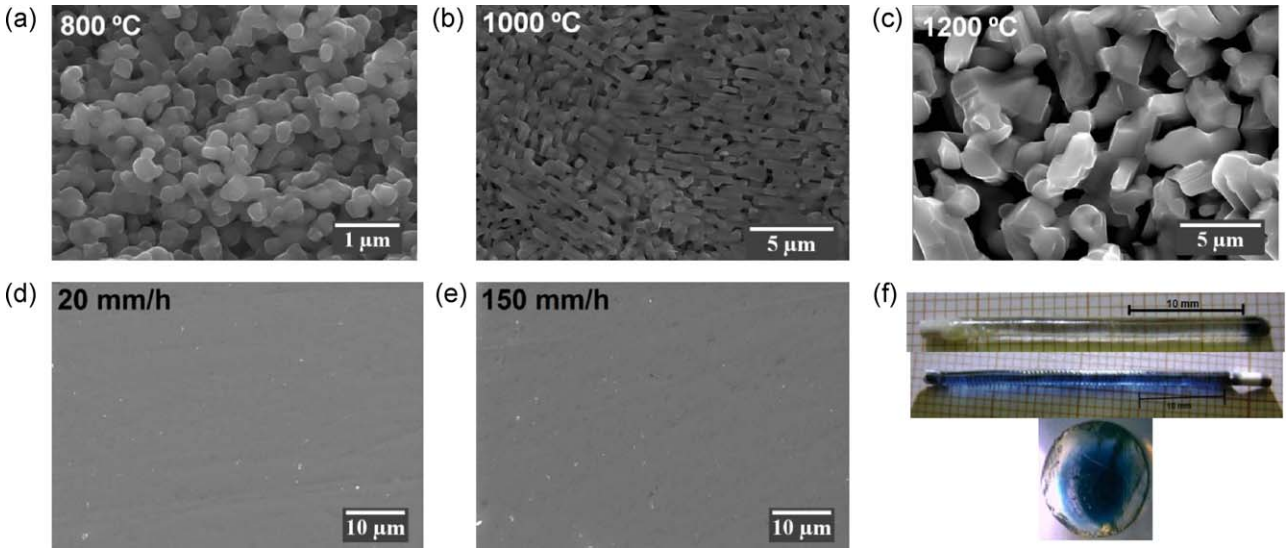

Fig. 2. SEM images, in secondary electron mode, of the sintered Nb_2O_5 pellets (a–c). SEM images, in secondary electron mode and photographs images of the LFZ grown fibres (d–f).

consequently, a decrease of the oxygen diffusion rate along the fibre diameter is plausible. The cross section picture presented in Fig. 2 shows this colour variation along the fibre radius, which is virtually colourless at the borders getting bluer near the centre. The fact that the slower fibre is completely colourless and free from the NbO_2 phase, unveils a possible relation between the blue colour, the NbO_2 phase and the growing rate. Both fibres present good morphological homogeneity without any visible bubbles, cracks or grain boundaries, as shown by the SEM images in Fig. 2.The LFZ grown fibres were analysed by optical absorption spectroscopy and PL measurements. In a similar way, the sintered pellets were studied by diffuse reflectance and photoluminescence. Fig. 3(a) shows the 14 K and RT optical absorption results performed along the growth axis direction for fibres grown at 20 mm/h and 150 mm/h. A linear relationship between $(\alpha d)^2$ and the photon energy occurs in agreement with the expected behaviour of a direct semiconductor bandgap (α stands for the absorption coefficient and d for the sample thickness). At low temperature the H-Nb_2O_5 fibres start to transmit light for energies below ~3.2 eV and a bandgap shrinkage of ~100 meV can be observed up to the RT. By exciting the fibres with photon energy above the measured bandgap (3.8 eV, He–Cd laser line excitation), no detectable luminescence was observed in the energy range between 1.45 eV and 3.0 eV. Conversely, with the same excitation energy, the sintered pellets show an unstructured broad-band luminescence in the orange-red spectral region as shown in Fig. 3(b). The defect from which the luminescence originates depends on the sintering temperature, as can be seen by the low energy shift of the PL peak position. The analysis of the PL recombination in a temperature range between 14 K and RT allows us to establish the luminescence thermal quenching. Assuming that the broad emission band is only due to an optical active centre, the competitive nonradiative relaxation mechanisms are well accounted by single activation energies of 12 meV and 40 meV for the samples sintered at 800 °C (T-Nb_2O_5) and 1200 °C (H-Nb_2O_5),

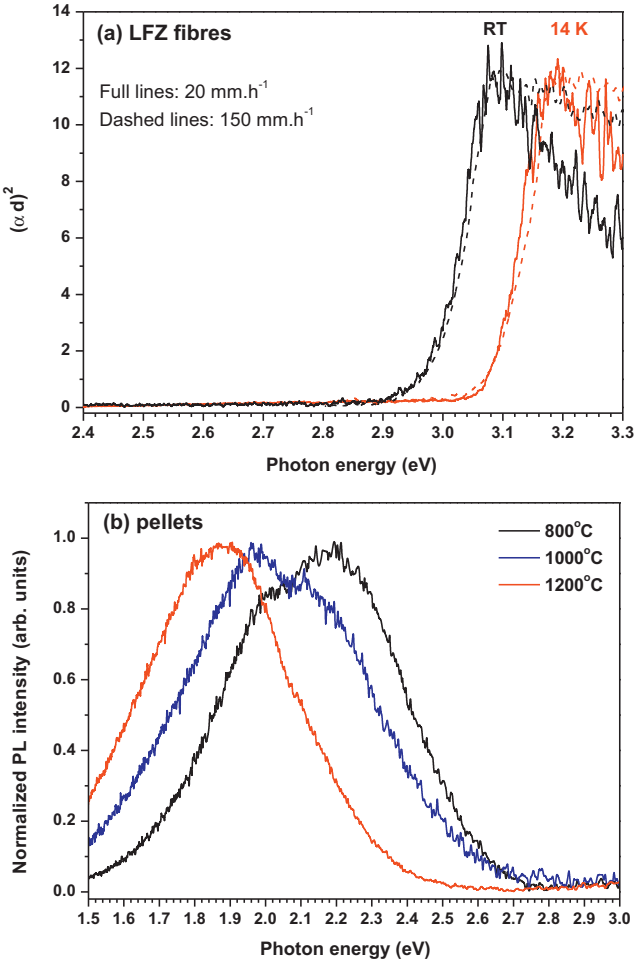

Fig. 3. (a) 14 K and RT absorption spectra of the LFZ grown fibres. (b) Normalized 14 K PL spectra of the sintered Nb_2O_5 pellets obtained with 3.8 eV excitation.

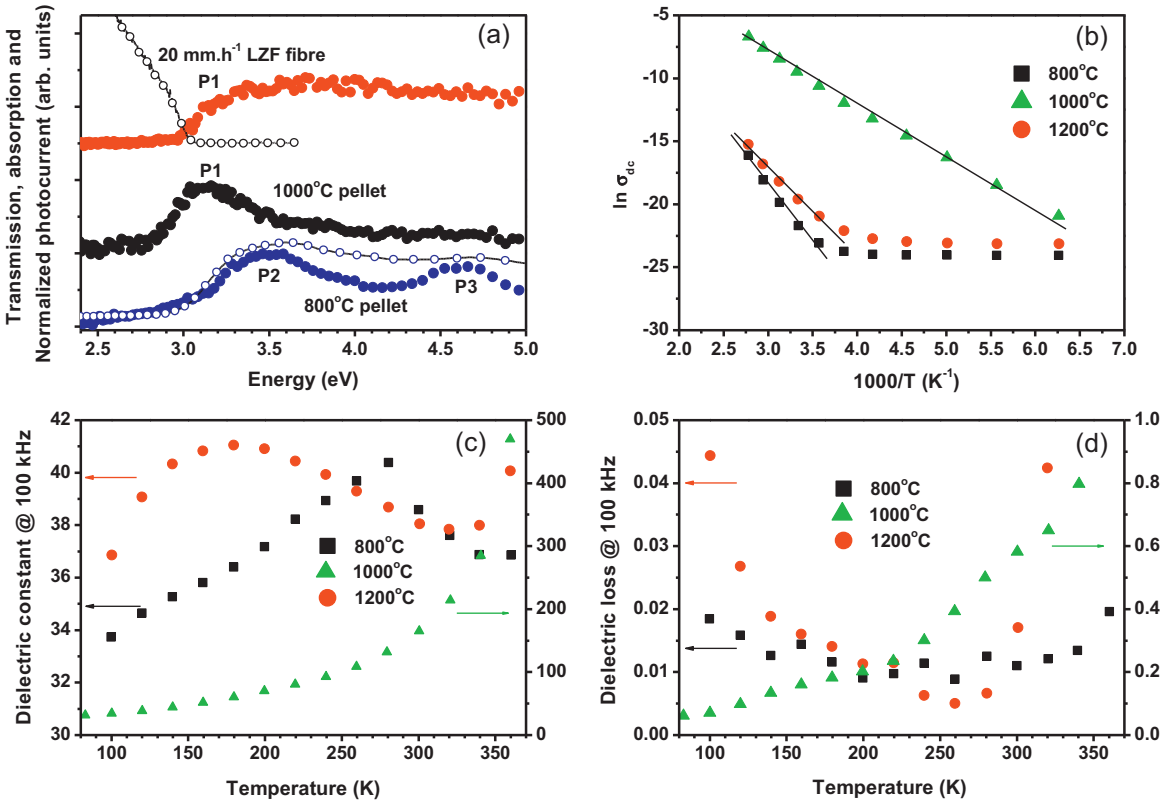

Fig. 4. (a) RT photoconductivity spectra of the fibre grown at 20 mm/h (red) and sintered pellets at 1000 °C (black) and 800 °C (blue). RT transmission and absorption spectra of the fibre and 800 °C pellet (dashed lines). Temperature dependence of (b) dc conductivity, (c) dielectric constant at 100 kHz and (d) dielectric loss for the sintered pellets. (For interpretation of the references to color in this figure legend, the reader is referred to the web version of the article.)

respectively. However, for the sample sintered at 1000 °C (H-Nb_2O_5), the nonradiative deexcitation processes are described by two activation energies of 3 meV and 40 meV.

Photoconductivity spectra at RT display different maxima P1, P2 and P3, at approximately 3.1, 3.5 and 4.7 eV which are dependent on the crystalline phase nature, as shown in Fig. 4(a). Comparing the PC spectra of the samples with the H-Nb_2O_5 crystalline phase (sintered pellet at 1000 °C and the fibre grown 20 mm/h) with the RT fibre transmission spectrum it can be observed that the peak P1 is located in the range of the fundamental band edge absorption. The decrease of the PC above the band edge seen, for instance, in the 1000 °C sintered pellet, comes from the decreasing of the penetration depth, due to the creation of more carriers near the surface where recombination could assume an important role. For the orthorhombic samples (T-Nb_2O_5) the P1 peak is absent and P2 and P3 peaks are detected. The P2 peak at 3.5 eV coincides with the reported bandgap energy in films produced by sol–gel with similar crystalline phase.[14] However, it is clear that in our samples sintered at 800 °C, an additional PC peak at 4.7 eV occurs which was also confirmed by the RT absorption measurements (dashed line in Fig. 4(a)). Assuming that the 3.5 eV corresponds to the fundamental absorption edge, the 4.7 eV band should also be of intrinsic origin. In this case, as happens in several semiconductor and insulator hosts,[15,16] the high energy intrinsic absorption could be related with transitions from different critical points in the conduction band for the orthorhombic Nb_2O_5 band structure. This was also observed for the orthorhombic V_2O_5 which has a band gap of 2.38 eV measured by optical absorption and reflectance.[17] Theoretical calculations[18] indicate the top of the valence band along the R-T direction and the bottom of the split-off conduction band at the Γ point. The direct band gap is expected to be localized at 1 eV above the indirect one.[18] On the other hand, variations in the reflectance as observed in other oxide hosts[19] are unlikely, since the PC and absorption spectra evidence the same peaks.

The electrical dc conductivity measurements show, for the samples sintered at 800 °C and 1200 °C, the existence of two different conducting mechanisms, one at temperatures lower than 200 K and the other for temperatures above it (Fig. 4(b)). In opposition, the sample sintered at 1000 °C shows only one conducting mechanism. Considering the high temperature range, this sample presents the lowest activation energy (0.37 eV), which suggests that the highest value of σ_{dc} can be related to a higher mobility of the charge carriers. The low value of the activation energy can be associated to the parallelepipedic morphology observed by SEM (Fig. 2), which presents a preferential grain orientation. This morphological characteristic is not as pronounced in the H-Nb_2O_5 sample sintered at 1200 °C, which could explain its higher activation energy (0.52 eV) and lower conductivity. The singular behaviour of the sample sintered at 1000 °C was confirmed for all the three sample batches

produced in this study.At RT and 100 kHz, the value of the dielectric constant (ε') is approximately 38 for samples sintered at 800 °C and 1200 °C increasing to 165 for the sample sintered at 1000 °C (Fig. 4(c)). The high value of ε' observed for this last sample is tentatively attributed to the preferential grain orientation which is expected to increase the dipole moment. Despite the high dielectric constant, a large dielectric loss value at RT ($\tan\delta \sim 0.58$) was calculated as shown in Fig. 4(d). In opposition, the sintered samples at 800 °C and 1200 °C exhibit a smaller dielectric loss ($\tan\delta < 0.02$) probably due to the absence of preferential grain orientation.

4. Conclusions

Nb_2O_5 sintered pellets were produced between 600 °C and 1200 °C in order to analyze their physical properties for potential applications in passive components. The crystalline phase nature of the as-produced samples has shown to be strongly dependent on the sintering temperature, an orthorhombic to monoclinic transformation being observed for temperatures higher than 800 °C. This transition is accompanied by a grain morphology change from nearly spherical to parallelepipedic shape.

Nb_2O_5 LFZ grown fibres produced with different growth rates have the same monoclinic crystal phase as that of the pellets sintered at high temperatures. A bandgap energy of ∼3.2 eV was found at 14 K, decreasing 100 meV up to the RT. In addition, the bandgap was confirmed by photoconductivity measurements. For sintered samples with orthorhombic phase, the presence of high energy absorption and photoconductivity peaks opens the possibility to the observation of indirect and direct band gap transitions as those observed for other transition metal ion oxides with similar crystalline structure.

Optically active centres on sintered samples with both crystalline phases were identified with UV excitation. Broad unstructured luminescence bands in the orange/red spectral region with different thermal quenching and with the peak position dependent of the sintering temperature were observed, whereas no luminescence was detected in the LFZ grown fibres.A dependence of the electrical properties with the morphology was observed, the sintered samples with preferential orientation of parallelepipedic grains exhibiting the highest dielectric constant value ($\varepsilon' \sim 165$).

Acknowledgements

The authors gratefully acknowledge the support from QREN/Compete – NbO (project no. 5309). We also acknowledge support from FCT, Portugal (PTDC/CTM/66195/2006). M. Peres thanks to FCT for his grant (SFRH/BD/45774/2008). The authors gratefully acknowledge M.R. Soares, N. Franco, P. Brandão, C. Azevedo for their technical support.

References

1. Sá AID, Rangel CM, Skeldon P. Semiconductive properties of anodic niobium oxides. *Portugaliae Electrochimica Acta* 2006;**24**(2):305–11.
2. Pozdeev Y. Reliability comparison of tantalum and niobium solid electrolytic capacitors. *Quality and Reliability Engineering International* 1998;**14**(2):79–82.
3. Störmer H, Weber A, Fischer V, Ivers-Tiffée E, Gerthsen D. Anodically formed oxide films on niobium: microstructural and electrical properties. *Journal of the European Ceramic Society* 2009;**29**(June (9)):1743–53.
4. Balachandran U, Eror NG. Raman spectrum of the high temperature form of Nb_2O_5. *Journal of Materials Science Letters* 1982;**1**(9):374–6.
5. Viet AL, Reddy MV, Jose R, Chowdari BVR, Ramakrishna S. Nanostructured Nb_2O_5 polymorphs by electrospinning for rechargeable lithium batteries. *The Journal of Physical Chemistry C* 2010;**114**(January (1)):664–71.
6. Braga V, Garcia F, Dias J, Dias S. Phase transition in niobium pentoxide supported on silica-alumina. *Journal of Thermal Analysis and Calorimetry* 2008;**92**(June (3)):851–5.
7. Vezzoli GC. Electrical properties of NbO_2 and Nb_2O_5 at elevated temperature in air and flowing argon. *Physical Review B* 1982;**26**(Out (7)):3954.
8. McConnell AA, Aderson JS, Rao CNR. Raman spectra of niobium oxides. *Spectrochimica Acta Part A: Molecular Spectroscopy* 1976;**32**(5):1067–76.
9. Nowak I, Ziolek M. Niobium compounds: preparation, characterization, and application in heterogeneous catalysis. *Chemical Reviews* 1999;**99**(Dez (12)):3603–24.
10. Adadurov GA, Breusov ON, Dremin AN, Dropyshev VN, Pershin SV. Phase transitions of shock-compressed T-Nb_2O_5 and H-Nb_2O_5. *Combustion Explosion and Shock Waves* 1974;**7**(4):503–6.
11. Brayner R, Bozon-Verduraz F. Niobium pentoxide prepared by soft chemical routes: morphology, structure, defects and quantum size effect. *Physical Chemistry Chemical Physics* 2003;**5**(7):1457–66.
12. Park JK, Kim KH, Tanaka I, Shim KB. Characteristics of rutile single crystals grown under two different oxygen partial pressures. *Journal of Crystal Growth* 2004;**268**(July (1–2)):103–7.
13. Higuchi M, Sato C, Kodaira K. High-speed float zone growth of rutile single crystals inclined at 48° to the *c*-axis. *Journal of Crystal Growth* 2004;**269**(Set (2–4)):342–6.
14. Barros Filho DA, Abreu Filho PP, Werner U, Aegerter MA. Photoelectrochemical properties of sol–gel Nb_2O_5 films. *Journal of Sol-Gel Science and Technology* 1997;**8**(Fev (1)):735–42.
15. Deb SK. Photoconductivity and photoluminescence in amorphous titanium dioxide. *Solid State Communications* 1972;**11**(June):713–5.
16. Cardona M, Gunther H. Optical properties and band structure of wurtzite-type crystals and rutile. *Physical Review* 1965;**137**(October (5A)):A1467–76.
17. Moshfegh AZ, Ignatiev A. Formation and characterization of thin film vanadium oxides: Auger electron spectroscopy, X-ray photoelectron spectroscopy, X-ray diffraction, scanning electron microscopy, and optical reflectance studies. *Thin Solid Films* 1991;**198**(September):251–68.
18. Goclon J, Grybos R, Witko M, Hafner Jürgen. Relative stability of low-index V_2O_5 surfaces: a density functional investigation. *Journal Physics: Condensed Matter* 2009;**21**(February):95008 (8 pp.).
19. Weinberg ZA, Rubloff GW, Bassous E. Transmission, photoconductivity, and the experimental band gap of thermally grow SiO_2 films. *Physical Review B* 1979;**19**(October (6)):3107–17.